10-23-2020

Optimal Control of Active Nematics

Michael M. Norton

Piyush Grover

Michael F. Hagan

Seth Fraden

Editors' Suggestion

Optimal Control of Active Nematics

Michael M. Norton*
Center for Neural Engineering, Department of Engineering Science and Materials, Pennsylvania State University, University Park, Pennsylvania 16801, USA
and Physics Department, Brandeis University, Waltham, Massachusetts 02453, USA

Piyush Grover
Mechanical and Materials Engineering, University of Nebraska—Lincoln, Lincoln, Nebraska 68588, USA

Michael F. Hagan
Physics Department, Brandeis University, Waltham, Massachusetts 02453, USA

Seth Fraden†
Physics Department, Brandeis University, Waltham, Massachusetts 02453, USA

(Received 26 July 2020; accepted 18 September 2020; published 23 October 2020)

In this work we present the first systematic framework to sculpt active nematic systems, using optimal control theory and a hydrodynamic model of active nematics. We demonstrate the use of two different control fields, (i) applied vorticity and (ii) activity strength, to shape the dynamics of an extensile active nematic that is confined to a disk. In the absence of control inputs, the system exhibits two attractors, clockwise and counterclockwise circulating states characterized by two co-rotating topological $+\frac{1}{2}$ defects. We specifically seek spatiotemporal inputs that switch the system from one attractor to the other; we also examine phase-shifting perturbations. We identify control inputs by optimizing a penalty functional with three contributions: total control effort, spatial gradients in the control, and deviations from the desired trajectory. This work demonstrates that optimal control theory can be used to calculate nontrivial inputs capable of restructuring active nematics in a manner that is economical, smooth, and rapid, and therefore will serve as a guide to experimental efforts to control active matter.

DOI: 10.1103/PhysRevLett.125.178005

Active matter represents a broad class of materials and systems comprising interacting and energy-consuming constituents. Systems ranging from cytoskeletal proteins to bird flocks are unified by their common ability to spontaneously manifest collective behaviors on a scale larger than the individual agents. One of the promises of active matter research is that it will enable the design of new self-organizing materials that possess the lifelike property of switching between distinct, robust, nontrivial dynamical states or configurations in response to external stimuli [1]. Towards rationally designing active materials with functional properties, we apply optimal control theory to an active nematic material, an important subclass of active matter that includes bacterial films and cell colonies [2], to switch the system between dynamical attractors in an optimally smooth, rapid, and efficient manner.

Here we present a concrete paradigm for applying optimal control to active matter. This theoretical work is motivated by a model experimental active matter system comprising microtubules and motor proteins that utilizes ATP fuel to slide microtubules and thereby generate extensile stress [3–5]. When compacted into a dense quasi-2D layer, these microtubules organize into a nematic with strong, local orientational order. Extensile stresses in active nematics drive instabilities that create motile topological defects and chaotic hydrodynamics [6–11]. In order to harness the chemomechanical abilities of these materials to do useful work, these dynamics need to be controlled [12]. Experimentally, this has been accomplished through physical means by introducing anisotropic friction to the underlying surface using liquid crystals [13,14], and through confinement within hardwall boundaries [15,16]. While these approaches can radically alter the dynamics, by corralling defects into lanes or regular trajectories, the potential for spatiotemporal actuation with these methods is limited. Recently, light-activated motor complexes have been created, allowing active stress to be spatiotemporally modulated by an external light source in microtubule gels [17] and nematics [18]. In these promising demonstrations, the control targets are relatively simple. This allows intuition, and trial and error, to inform suitable *ad hoc* control inputs. However, to systematically achieve more elaborate configuration goals, a framework is needed that includes a dynamical model of the system.

To that end, we consider the problem of driving an active nematic between two attractors, by formally applying

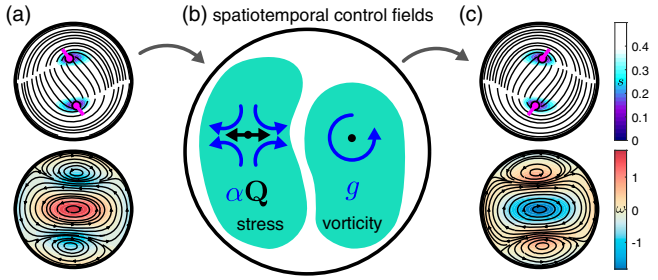

FIG. 1. (a) Director $\mathbf{n}$ with degree of order s and defects in magenta (top) and flow field $\mathbf{u}$ with vorticity ω (bottom), for initial condition in the counterclockwise circulating attractor. (b) Schematic showing two modes of control input. (c) Director and flow field of the clockwise target configuration.

optimal control theory to a nematohydrodynamic model and solving for the necessary control inputs. Our control goal is therefore not to regulate or stabilize the system, but instead to steer the system between two distinct configurations in a manner that is optimally smooth, efficient, and rapid. We consider separately two spatiotemporal control fields: (i) an applied rotation rate $g(\mathbf{x}, t)$ that rotates the nematic director $\mathbf{Q}$ directly, and (ii) the active stress strength $\alpha(\mathbf{x}, t)$ which acts through the momentum equation and experimentally can be controlled through light input [17,18]. The former does not currently have an experimental analog but nothing in principle prevents engineering such a control field.

We consider an active nematic already corralled by confinement in a disk with strong parallel anchoring and no-slip boundary conditions, such that it does not exhibit chaotic dynamics [19]. Instead, the system produces two stable limit cycle attractors characterized by two, motile $+\frac{1}{2}$ disclinations that perpetually orbit the domain at fixed radius in either the clockwise or counterclockwise direction; note the handedness of the defect configurations in Fig. 1(a) and 1(c). That is, these attractors are mirror images of each other, a consequence of the system dynamics' equivariance under reflection. While these are steady states of the system, they are maintained by a constant flux of energy through the extensile active stress and are therefore minimal, self-organized attractors of the material. In the absence of activity, the director field would relax to a motionless equilibrium configuration. As an exemplar application of optimal control theory, we have identified the spatiotemporal actuation of either applied vorticity or active stress that rearranges the nematic director field and moves the system from one attractor to the other, while optimally balancing the amount of control input against the penalty for deviations from the target configuration (Figs. 2 and 4, and movies S1 and S2 in the Supplemental Material [20]). This is akin to the process of gait switching in neuroscience. It has been shown that even small networks of oscillators are capable of multiple rhythms that are accessible through external inputs [21,22]. We also consider phase-shifting perturbations within one attractor using both control fields; movies S3 and S4 in the Supplemental Material [20].

Nematohydrodynamic model.—We utilize a previously explored continuum nematohydrodynamic model [19,23], which we restate here in dimensionless form. We choose this model for simplicity but note that other models can be put into the same control framework [8,24]. As a minimal representation of our system, we use an incompressible, single-fluid model whose state is described by the dimensionless nematic order tensor $\mathbf{Q} = s\rho[\mathbf{n} \otimes \mathbf{n} - (1/2)\mathbf{I}]$ and

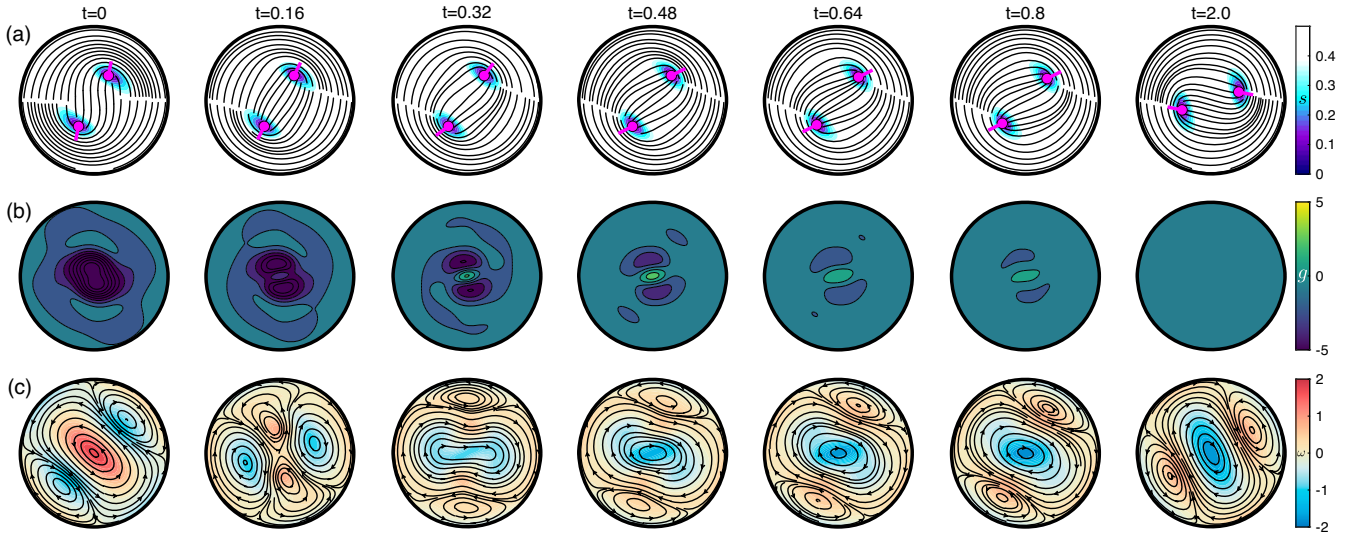

FIG. 2. Transformation from counterclockwise to clockwise rotation using applied vorticity actuation. (a) Director field and degree of order, (b) applied vorticity $g(\mathbf{x}, t)$ and (c) velocity field and vorticity, with $W = 600$, $t_f = 2$. See movie S1 in the Supplemental Material [20].

fluid flow field $\mathbf{u}$. $\mathbf{Q}$ describes both the local orientation $\mathbf{n}$ and degree of order s of the nematic, and is scaled by the nematic density ρ such that ($\rho s = \sqrt{2\mathrm{Tr}\mathbf{Q}^2}$). The coupled dynamics are given by

$$\partial_t \mathbf{Q} + \nabla\cdot(\mathbf{u}\mathbf{Q}) - [(\mathbf{\Omega}+\mathbf{G})\mathbf{Q} - \mathbf{Q}(\mathbf{\Omega}+\mathbf{G})] - \lambda\mathbf{E} - \mathbf{H} = f_{\mathbf{Q}}(\mathbf{Q},\mathbf{u},g) = 0 \quad (1)$$

Along the boundary $\mathbf{Q}|_{\partial\Omega} = s^*\rho[\mathbf{t}\otimes\mathbf{t} - (1/2)\mathbf{I}]$, with boundary tangent $\mathbf{t}$ and degree of order $s^* = \sqrt{2}$ associated with a fully ordered nematic in the limit $\rho\to\infty$ [25]. Kinematic terms and free-energy relaxation both contribute to the dynamics of $\mathbf{Q}$. The kinematic terms depend on the local fluid flow velocity and gradients, with $\Omega_{ij} = \frac{1}{2}(\partial_j u_i - \partial_i u_j)$ as the antisymmetric vorticity tensor and $E_{ij} = \frac{1}{2}(\partial_j u_i + \partial_i u_j)$ as the symmetric strain rate tensor. The vorticity tensor is augmented by an applied field $\mathbf{G} = \frac{1}{2}\left(\begin{smallmatrix}0 & -g\\ g & 0\end{smallmatrix}\right)$, where g is one of the control inputs we consider, applied vorticity. The relaxational terms $\mathbf{H}$ are proportional to variations of the system free energy, $\mathbf{H} = (\beta_1 - \beta_2\mathbf{Q}:\mathbf{Q})\mathbf{Q} + 2\nabla^2\mathbf{Q}$. Momentum conservation in the Stokes limit, incompressibility constraint $\nabla\cdot\mathbf{u} = 0$, and boundary conditions $\mathbf{u}|_{\partial\Omega} = 0$ govern the fluid flow

$$\eta\nabla^2\mathbf{u} - \nabla P - \nabla\cdot(\alpha\mathbf{Q}) = f_{\mathbf{u}}(\mathbf{Q},\mathbf{u},\alpha) = 0, \quad (2)$$

with pressure P and strength of activity α. The active stress, $-\alpha\mathbf{Q}$ corresponds to an extensile dipole force density [2,26,27]. The scaling factor α serves as the second form of spatiotemporal control input that we consider. Since $\mathbf{Q}\propto\rho$, relaxing the uniform density assumption would add nuance to the dynamics and control by allowing $\nabla\rho$ to drive flow [25,28,29]. Systems with an isotropic active stress component, such as growing bacterial colonies, contain additional terms [30]. In some applications, control of $\rho(\mathbf{x},t)$ itself may be of interest.

Optimal control.—We seek a spatiotemporal input field, either $g(\mathbf{x},t)$ or $\alpha(\mathbf{x},t)$, that drives the system towards a desired director field configuration $\mathbf{Q}^*$ by minimizing the following scalar cost functional $\mathcal{J}$

$$\mathcal{J} = \frac{1}{2}\int_0^{t_f} dt \int_\Omega d^2\mathbf{x}\Big[g^2 + \Gamma_g\nabla g\cdot\nabla g + (\alpha-\alpha_0)^2 + \Gamma_\alpha\nabla\alpha\cdot\nabla\alpha + W\frac{1}{2}\Delta\mathbf{Q}:\Delta\mathbf{Q}\Big], \quad (3)$$

subject to Eq. (1) and Eq. (2). We pose the control problem as a tracking problem by quadratically penalizing deviations $\Delta\mathbf{Q} = \mathbf{Q}(\mathbf{x},t) - \mathbf{Q}^*(\mathbf{x},\theta+t-t_f)$ from the desired state throughout the control window $t\in[0,t_f]$. $\mathbf{Q}^*$ is selected from a precalculated time-periodic solution, Fig. 1. We shift the lookup of $\mathbf{Q}^*$ continuously in time such that at the end of the control window, the time of the reference solution is θ. Control actuation is also penalized quadratically with either $(\alpha-\alpha_0)^2$ or g^2. We penalize deviations from α_0 rather than α itself to maintain the intrinsic dynamics of the material as much as possible. Finally, we promote smoothness on α and g by additionally penalizing $\nabla\alpha\cdot\nabla\alpha$ and $\nabla g\cdot\nabla g$, with weights Γ_α and Γ_g. This is more crucial when α is the control input, since gradients in α can be exploited to achieve arbitrarily large forces, which we want to discourage. Including these three penalties creates a control problem with opposing forces; the solutions we identify optimally balance matching the desired trajectory quickly against applying inputs to the system. We can sacrifice accuracy but use less control by decreasing the weight W on the state penalty, or alternatively arrive more rapidly at the target configuration by increasing W.

Following Pontryagin's theorem [31,32], we constrain our search of optimal state trajectories to those that obey the system dynamics by introducing Lagrange multipliers $\boldsymbol{\psi}(\mathbf{x},t)\in\mathbb{R}^{2\times2}$, $\boldsymbol{\nu}(\mathbf{x},t)\in\mathbb{R}^2$, and $\phi(\mathbf{x},t)\in\mathbb{R}^1$, which are the adjoint or costate variables for $\mathbf{Q}$, $\mathbf{u}$, and P, respectively, and augmenting the original cost function Eq. (3) to give $\mathcal{L} = \mathcal{J} + \int_0^{t_f} dt\int_\Omega d^2\mathbf{x}[\boldsymbol{\nu}\cdot\mathbf{f}_{\mathbf{u}} + \boldsymbol{\psi}:\mathbf{f}_{\mathbf{Q}} + \phi(\nabla\cdot\mathbf{u})]$. The conditions for optimality are $(\delta\mathcal{L}/\delta\boldsymbol{\psi})$, $(\delta\mathcal{L}/\delta\boldsymbol{\nu})$, $(\delta\mathcal{L}/\delta\phi)$, $(\delta\mathcal{L}/\delta\mathbf{Q})$, $(\delta\mathcal{L}/\delta\mathbf{u})$, $(\delta\mathcal{L}/\delta P)$, $(\delta\mathcal{L}/\delta\alpha)$, $(\delta\mathcal{L}/\delta g) = 0$. The first three conditions simply return the original nematohydrodynamic equations governing $\{\mathbf{Q},\mathbf{u},P\}$, Eq. (1) and Eq. (2). The following three conditions yield the dynamical equations for the adjoint variables $\{\boldsymbol{\psi},\boldsymbol{\nu},\phi\}$:

$$-\nabla^2\boldsymbol{\nu} - \nabla\phi + \mathbf{h}_1 = 0, \nabla\cdot\boldsymbol{\nu} = 0 \quad (4)$$

$$W(\mathbf{Q}-\mathbf{Q}^*) - \partial_t\boldsymbol{\psi} - \mathbf{u}\cdot\nabla\boldsymbol{\psi} - 2\nabla^2\boldsymbol{\psi} + \alpha\mathbf{h}_2 + g\mathbf{h}_3 + \mathbf{h}_4 + 2\mathbf{Q}\beta_2(\mathbf{Q}:\boldsymbol{\psi}) - \boldsymbol{\psi}(\beta_1 - \beta_2\mathbf{Q}:\mathbf{Q}) = 0, \quad (5)$$

with final conditions $\{\boldsymbol{\nu},\boldsymbol{\psi}\}(\mathbf{x},t_f) = 0$ and boundary conditions $\{\boldsymbol{\nu},\boldsymbol{\psi}\}|_{\partial\Omega} = 0$. Full expressions for the terms $\mathbf{h}_{1-4}$ are stated in Ref. [33], where we have used Q_{xy}, $\psi_{xy} = Q_{yx}$, ψ_{yx} and Q_{xx}, $\psi_{xx} = -Q_{yy}$, ψ_{yy}. The final two optimality conditions $(\delta\mathcal{L}/\delta\alpha), (\delta\mathcal{L}/\delta g) = 0$ constrain the control inputs:

$$(\alpha-\alpha_0) - \Gamma_\alpha\nabla^2\alpha - [Q_{xx}(\partial_x\nu_x - \partial_y\nu_y) + Q_{xy}(\partial_y\nu_x + \partial_x\nu_y)] = 0 \quad (6)$$

$$g - \Gamma_g\nabla^2 g + (Q_{xy}\psi_{xx} - Q_{xx}\psi_{xy}) = 0. \quad (7)$$

Additional degrees of freedom, such as the nematic density ρ in a compressible system, can readily be included by introducing concomitant adjoint variables and optimality conditions.

We solve the coupled PDE system and constraints using the direct-adjoint-looping method [34]; our code is

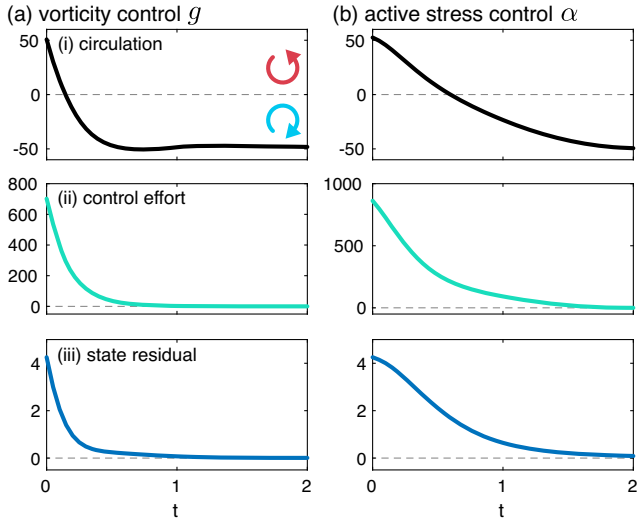

FIG. 3. Evolution of bulk system properties during counterclockwise to clockwise maneuvers using (a) vorticity control $g(\mathbf{x},t)$, Fig. 2, and (b) active stress strength $\alpha(\mathbf{x},t)$, Fig. 4: (i) circulation $\int_\Omega d^2\mathbf{x}\mathbf{u}\cdot\hat{\mathbf{e}}_\theta$, control effort for (a) $\frac{1}{2}\int_\Omega d^2\mathbf{x}g^2$ or (b) $\frac{1}{2}\int_\Omega d^2\mathbf{x}(\alpha-\alpha_0)^2$, and (iii) residual between the system state and target $\frac{1}{4}\int_\Omega d^2\mathbf{x}\Delta\mathbf{Q}:\Delta\mathbf{Q}$.

available at Refs. [35,36]. We consecutively solve the forward dynamics Eq. (1) and Eq. (2), and adjoint dynamics Eq. (5) and Eq. (4). The latter are solved backwards in time and thus are responsible for propagating the residuals of the director field $\Delta\mathbf{Q}$. After each backward run, the control fields are updated via gradient descent using the Eq. (7) for applied vorticity or Eq. (6) for stress. Gradient descent step sizes are chosen using the Armijo backtracking method [37]. The process is repeated until the cost function Eq. (3) converges to a desired tolerance $\sim 10^{-4}$. For all computations $\lambda = 1$ and $\Gamma_{g,\alpha} = 0.1$. We restrict ourselves to a domain size of radius $R = 6.5$ and baseline active stress $\alpha_0 = 5$ that produces a stable periodic solution consisting of a single fluid vortex driven by two $+\frac{1}{2}$ defects (Fig. 1) [19]. Both clockwise and counterclockwise circulating states are precalculated and used as $\mathbf{Q}^*$ and initial conditions. The state and adjoint fields are integrated using the finite element analysis software COMSOL [35,36].

Results.—We first consider chirality switching using applied vorticity g, see Fig. 2 and movie S1 in the Supplemental Material [20]. At $t = 0$ the applied control field (second row) is strongest in the center of the disk and opposes the native vorticity (last row). The amplitude of the control quickly fades as the director field (first row) transitions through a symmetric, dipolar configuration ($t = 0.16$) to the other attractor. After the defects begin circulating in the desired clockwise direction, small amounts of control are applied to adjust the director field so that it matches the target trajectory (movies S1–S4 [20] all show both the solution $\mathbf{Q}$ and target $\mathbf{Q}^*$ for reference). We next consider the same control goal using the activity strength α as the input, Fig. 4. In this case a combination of strong extensile and weak contractile stresses are used to again pull the defects towards the dipolar configuration ($t = 0.96$) and then nudge them towards the other attractor. Figure 3 summarizes the dynamics of the system for both vorticity and stress control by plotting the evolution of three spatially integrated quantities: (i) circulation, which coarsely describes the proximity of the system to one of the circulating attractors (note that the zero crossing coincides with the system's transition through the achiral configuration), (ii) control effort, and (iii) residual of the director that measures the approach of the system $\mathbf{Q}$ to the target trajectory $\mathbf{Q}^*$.

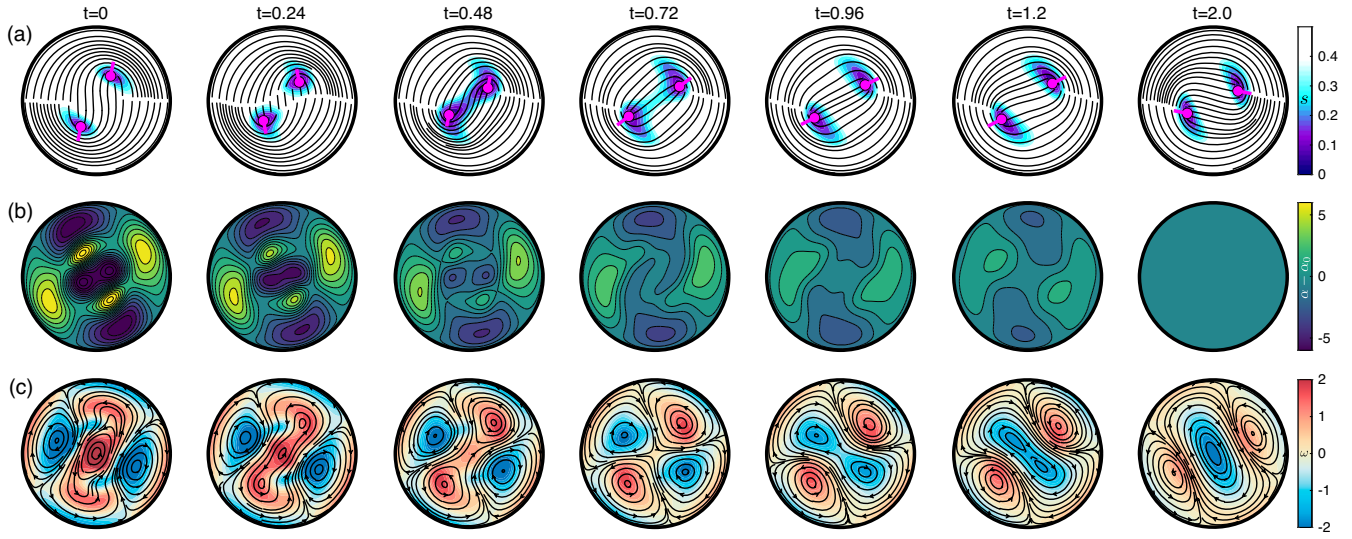

FIG. 4. Transformation from counterclockwise to clockwise rotation using active stress actuation, (a) director field and degree of order, (b) active stress $\alpha(\mathbf{x},t)-\alpha_0$, and (c) velocity field and vorticity, $W = 900$, $t_f = 2$. See movie S2 in the Supplemental Material [20].

We next consider phase-shifting maneuvers actuated by vorticity (movie S3 [20]) and stress (movie S4 [20]). In the former, additional positive vorticity is applied to the interior of the disk, between the two $+\frac{1}{2}$ defects, while negative vorticity is applied in two regions at larger radii. These regions of opposing applied vorticity act on either side of the defects like enmeshed gears, to rapidly advance the position of the defects and thus the phase. This action adds noticeable twist to the director ($t = 0.24$) that relaxes once the control fades. In the latter, additional active stresses are added at large radii, stopping circulation and temporarily moving the director to a symmetric, dipolar, configuration ($t = 0.68$), similar to the action seen in the attractor-switching maneuver explored in Fig. 4 and movie S2 in the Supplemental Material [20]. Active stresses then break the symmetry to resume circulation at the desired phase.

For both chirality switching and phase shifting, given the periodic nature of the starting and target configurations, it is likely that multiple solutions exist. For example, for every phase-advancing solution, there is likely a phase-delaying solution that achieves the same goal. This situation becomes more complex when switching between attractors and the phases of each attractor come into play. Thus, while we have used an optimal control framework, we cannot guarantee that the solutions found are globally optimal when multiple solutions exist; in this sense the control framework provides a means to generate *a* physically informed and plausible control solution. We speculate that isochron and isostable reduction of the full order control problem may yield physical insights and permit exploring the range of control scenarios more effectively [38–40]. Creating a more parsimonious model would also reduce computational time, easing experimental implementation.

Conclusion.—A grand challenge in active matter is to develop systems built from simple building blocks that manifest pre-programmed spatiotemporal dynamics [12]. The two circulating states we explore are emergent dynamical attractors that spontaneously self-assemble from an active liquid crystal when parameters are tuned correctly. This work paradigmatically demonstrates that one attractor can be effectively *reassembled* into a *new* attractor through the proper choice of system inputs.

While the active nature of the fluid we consider here gives rise to dynamics fundamentally different than those of driven, passive fluids, connections can be made between our work and control of classical turbulence. The attractors we explore are examples of exact coherent structures (ECSs), which are typically exact solutions to the Navier-Stokes equations. The dynamics of a turbulent flow can be thought of as a meandering path that visits multiple ECSs through heteroclinic connections [41,42]. While we have applied perturbations to switch basins of two attractors, one could envision a similar class of control problems that aim to stabilize certain ECSs or remove connecting orbits between ECSs to delay transition to the chaotic or (mesoscale) turbulent regime in active nematic systems [16,43]. Further, while we explored spatio-temporally smooth control inputs, changing the norm on the control penalty can be used to promote sparsity, resulting in control inputs that are spatially or temporally localized [44].

In addition to artificial active systems, living systems also present a potential application of control theory [32]. For example, stress gradients radically rearrange cells during embryonic development [45] and wound healing [46–48]. One can use the inverse problem framework of optimal control to design the stress fields necessary to achieve a particular morphological change, thereby guiding both experimental and medical device design.

This work was supported by the NSF MRSEC-1420382, NSF-DMR-2011486, NSF-DMR-1810077, and NSF-DMR-1855914 (M. M. N., M. F. H., and S. F.). P. G. was supported by UNL startup fund. Computational resources were provided by the NSF through XSEDE computing resources (MCB090163) and the Brandeis HPCC, which is partially supported by NSF-DMR-2011486. We thank Aparna Baskaran and Chaitanya Joshi for their helpful discussions.

*mike.m.norton@gmail.com
†fraden@brandeis.edu

[1] D. Needleman and Z. Dogic, Active matter at the interface between materials science and cell biology, Nat. Rev. Mater. **2**, 17048 (2017).
[2] M. C. Marchetti, J. F. Joanny, S. Ramaswamy, T. B. Liverpool, J. Prost, M. Rao, and R. A. Simha, Hydrodynamics of soft active matter, Rev. Mod. Phys. **85**, 1143 (2013).
[3] T. Sanchez, D. T. N. Chen, S. J. Decamp, M. Heymann, and Z. Dogic, Spontaneous motion in hierarchically assembled active matter, Nature (London) **491**, 431 (2012), https://github.com/wearefor/activenematic_oc.
[4] S. J. DeCamp, G. S. Redner, A. Baskaran, M. F. Hagan, and Z. Dogic, Orientational order of motile defects in active nematics, Nat. Mater. **14**, 1110 (2015).
[5] L. M. Lemma, M. M. Norton, S. J. DeCamp, S. A. Aghvami, S. Fraden, M. F. Hagan, and Z. Dogic, Multiscale dynamics in active nematics, arXiv:2006.15184.
[6] L. Giomi, Geometry, and Topology of Turbulence in Active Nematics, Phys. Rev. X **5**, 031003 (2015).
[7] A. Doostmohammadi, M. F. Adamer, S. P. Thampi, and J. M. Yeomans, Stabilization of active matter by flow-vortex lattices and defect ordering, Nat. Commun. **7**, 10557 (2016).
[8] T. Gao, M. D. Betterton, A.-S. Jhang, and M. J. Shelley, Analytical structure, dynamics, and coarse graining of a kinetic model of an active fluid, Phys. Rev. Fluids **2**, 093302 (2017).

[9] S. Chen, P. Gao, and T. Gao, Dynamics and structure of an apolar active suspension in an annulus, J. Fluid Mech. **835**, 393 (2018).

[10] A. Sokolov, A. Mozaffari, R. Zhang, J. J. de Pablo, and A. Snezhko, Emergence of Radial Tree of Bend Stripes in Active Nematics, Phys. Rev. X **9**, 031014 (2019).

[11] B. Martínez-Prat, J. Ignés-Mullol, J. Casademunt, and F. Sagués, Selection mechanism at the onset of active turbulence, Nat. Phys. **15**, 362 (2019).

[12] G. Gompper *et al.*, The 2020 motile active matter roadmap, J. Phys. Condens. Matter **32**, 193001 (2020).

[13] P. Guillamat, J. Ignés-mullol, and F. Sagués, Control of active liquid crystals with a magnetic field, Proc. Natl. Acad. Sci. U.S.A. **113**, 5498 (2016).

[14] P. Guillamat, J. Ignés-Mullol, and F. Sagués, Taming active turbulence with patterned soft interfaces, Nat. Commun. **8**, 564 (2017).

[15] J. Hardoüin, R. Hughes, A. Doostmohammadi, J. Laurent, T. Lopez-Leon, J. M. Yeomans, J. Ignés-Mullol, and F. Sagués, Reconfigurable flows and defect landscape of confined active nematics, Commun. Phys. **2**, 121 (2019).

[16] A. Opathalage, M. M. Norton, M. P. N. Juniper, B. Langeslay, S. A. Aghvami, S. Fraden, and Z. Dogic, Self-organized dynamics and the transition to turbulence of confined active nematics, Proc. Natl. Acad. Sci. U.S.A. **116**, 4788 (2019).

[17] T. D. Ross, H. J. Lee, Z. Qu, R. A. Banks, R. Phillips, and M. Thomson, Controlling organization and forces in active matter through optically defined boundaries, Nature (London) **572**, 224 (2019).

[18] R. Zhang, S. A. Redford, P. V. Ruijgrok, N. Kumar, A. Mozaffari, S. Zemsky, A. R. Dinner, V. Vitelli, Z. Bryant, M. L. Gardel, and J. J. de Pablo, Structuring stress for active materials control, arXiv:1912.01630.

[19] M. M. Norton, A. Baskaran, A. Opathalage, B. Langeslay, S. Fraden, A. Baskaran, and M. F. Hagan, Insensitivity of active nematic liquid crystal dynamics to topological constraints, Phys. Rev. E **97**, 012702 (2018).

[20] See Supplemental Material at http://link.aps.org/supplemental/10.1103/PhysRevLett.125.178005 for movies and movie descriptions.

[21] A. L. Shilnikov, Key bifurcations of bursting polyrhythms in 3-cell central pattern generators, PLoS One **9**, e92918 (2014).

[22] M. Lodi, A. L. Shilnikov, and M. Storace, Design principles for central pattern generators with preset rhythms, IEEE Trans. Neural Networks Learn. Syst. **31**, 1 (2019).

[23] A. N. Beris and B. J. Edwards, *Journal of Chemical Education* (Oxford University, New York, 1994), Vol. 36.

[24] S. Thampi and J. Yeomans, Active turbulence in active nematics, Eur. Phys. J. Spec. Top. **225**, 651 (2016).

[25] E. Putzig, G. S. Redner, A. Baskaran, and A. Baskaran, Instabilities, defects, and defect ordering in an overdamped active nematic, Soft Matter **12**, 3854 (2016).

[26] R. A. Simha and S. Ramaswamy, Hydrodynamic Fluctuations and Instabilities in Ordered Suspensions of Self-Propelled Particles, Phys. Rev. Lett. **89**, 058101 (2002).

[27] S. P. Thampi, R. Golestanian, and J. M. Yeomans, Vorticity, defects and correlations in active turbulence, Phil. Trans. R. Soc. A **372**, 20130366 (2014).

[28] M. L. Blow, S. P. Thampi, and J. M. Yeomans, Biphasic, Lyotropic, Active Nematics, Phys. Rev. Lett. **113**, 248303 (2014).

[29] A. Doostmohammadi, S. P. Thampi, and J. M. Yeomans, Defect-Mediated Morphologies in Growing Cell Colonies, Phys. Rev. Lett. **117**, 048102 (2016).

[30] D. Dell'Arciprete, M. L. Blow, A. T. Brown, F. D. Farrell, J. S. Lintuvuori, A. F. McVey, D. Marenduzzo, and W. C. Poon, A growing bacterial colony in two dimensions as an active nematic, Nat. Commun. **9**, 1 (2018).

[31] D. Kirk, *Optimal Control Theory: An Introduction* (Dover, Englewood Cliffs, New Jersey, 1970).

[32] S. Lenhart and J. T. Workman, *Optimal Control Applied to Biological Models* (Chapman and Hall/CRC, New York, 2007).

[33] $h_{1x} = \psi_{xx}\partial_x Q_{xx} + \psi_{xy}\partial_x Q_{xy} + \partial_y(Q_{xy}\psi_{xx} - Q_{xx}\psi_{xy}) + \lambda(\partial_x\psi_{xx} + \partial_y\psi_{xy}/2)$, $h_{1y} = \psi_{xx}\partial_y Q_{xx} + \psi_{xy}\partial_y Q_{xy} + \partial_x(Q_{xx}\psi_{xy} - Q_{xy}\psi_{xx}) + \lambda\partial_x\psi_{xy}/2$, $h_{2x} = \partial_y\nu_y - \partial_x\nu_x$, $h_{2y} = -(\partial_y\nu_x + \partial_x\nu_y)$, $h_{3x} = -\psi_{xy}$, $h_{3y} = \psi_{xx}$, $h_{4x} = \psi_{xy}(\partial_y u_x - \partial_x u_y)$, $h_{4y} = \psi_{xx}(\partial_x u_y - \partial_y u_x)$.

[34] R. R. Kerswell, C. C. Pringle, and A. P. Willis, An optimization approach for analysing nonlinear stability with transition to turbulence in fluids as an exemplar, Rep. Prog. Phys. **77**, 085901 (2014).

[35] M. M. Norton, activenematic_oc, GitHub Repository (2020) https://github.com/wearefor/activenematic_oc.

[36] M. M. Norton, Active nematic optimal control, OSF Project (2020) https://doi.org/10.17605/OSF.IO/QYK9T.

[37] A. Borzì and V. Schulz, *Computational Optimization of Systems Governed by Partial Differential Equations* (Society for Industrial and Applied Mathematics, Philadelphia, 2012).

[38] D. Wilson and J. Moehlis, Extending phase reduction to excitable media: Theory and applications, SIAM Rev. **57**, 201 (2015).

[39] B. Monga, D. Wilson, T. Matchen, and J. Moehlis, Phase reduction and phase-based optimal control for biological systems: A tutorial, Biol. Cybern. **113**, 11 (2019).

[40] D. Wilson and S. Djouadi, Isostable reduction and boundary feedback control for nonlinear convective flows, in *IEEE 58th Conference on Decision and Control (CDC), Nice, France,* (2019), p. 2138, https://ieeexplore.ieee.org/document/9029951.

[41] B. Suri, J. Tithof, R. O. Grigoriev, and M. F. Schatz, Forecasting Fluid Flows Using the Geometry of Turbulence, Phys. Rev. Lett. **118**, 114501 (2017).

[42] B. Suri, J. Tithof, R. O. Grigoriev, and M. F. Schatz, Unstable equilibria and invariant manifolds in quasi-two-dimensional Kolmogorov-like flow, Phys. Rev. E **98**, 023105 (2018).

[43] A. Doostmohammadi, T. N. Shendruk, K. Thijssen, and J. M. Yeomans, Onset of meso-scale turbulence in active nematics, Nat. Commun. **8**, 15326 (2017).

[44] C. Ryll, J. Löber, S. Martens, H. Engel, and F. Tröltzsch, Analytical, optimal, and sparse optimal control of traveling wave solutions to reaction-diffusion systems, Understand.

Complex Syst. **0**, 189 (2016), https://link.springer.com/chapter/10.1007/978-3-319-28028-8_10.

[45] S. J. Streichan, M. F. Lefebvre, N. Noll, E. F. Wieschaus, and B. I. Shraiman, Global morphogenetic flow is accurately predicted by the spatial distribution of myosin motors, eLife **7**, e27454 (2018).

[46] D. J. Cohen, W. J. Nelson, and M. M. Maharbiz, Galvanotactic control of collective cell migration in epithelial monolayers, Nat. Mater. **13**, 409 (2014).

[47] T. Turiv, J. Krieger, G. Babakhanova, H. Yu, S. V. Shiyanovskii, Q.-H. Wei, M.-H. Kim, and O. D. Lavrentovich, Topology control of human fibroblast cells monolayer by liquid crystal elastomer, Sci. Adv. **6**, eaaz6485 (2020).

[48] T. J. Zajdel, G. Shim, L. Wang, A. Rossello-Martinez, and D. J. Cohen, SCHEEPDOG: Programming electric cues to dynamically herd large-scale cell migration, Cell Syst. **10**, 506 (2020).